EMBO reports

scientific report

The structure of the flock house virus B2 protein, a viral suppressor of RNA interference, shows a novel mode of double-stranded RNA recognition

Andreas Lingel, Bernd Simon, Elisa Izaurralde[+] *& Michael Sattler*[++]
European Molecular Biology Laboratory, Heidelberg, Germany

We report the structure of the flock house virus B2 protein, a potent suppressor of RNA interference (RNAi) in animals and plants. The B2 protein is a homodimer in solution and contains three α-helices per monomer. Chemical shift perturbation shows that an antiparallel arrangement of helices (α2/α2′) forms an elongated binding interface with double-stranded RNA (dsRNA). This implies a novel mode of dsRNA recognition and provides insights into the mechanism of RNAi suppression by B2.

Keywords: RNAi; viral suppressor; dsRNA recognition
EMBO reports (2005) **6**, 1149–1155. doi:10.1038/sj.embor.7400583

INTRODUCTION

RNA silencing is thought to have originated from an ancient cellular defence mechanism against viral and other endogenous double-stranded RNAs (dsRNAs; Plasterk, 2002; Roth *et al*, 2004; Voinnet, 2005). This antiviral response is mediated by the cellular RNA interference (RNAi) machinery and targets viral transcripts for degradation using short interfering RNAs (siRNAs). To counteract this host cell defence mechanism, many viruses have evolved proteins that suppress RNA silencing. Flock house virus (FHV) belongs to Nodaviridae, a family of RNA viruses with a genome comprising two positive sense RNAs (Johnson *et al*, 2001). Recently, it was shown that FHV replication, which involves dsRNA molecules as intermediates, triggers a potent antiviral silencing response in *Caenorhabditis elegans*. This response requires the Argonaute protein rde-1, which is essential for RNAi mediated by siRNAs, but not by microRNAs (Lu *et al*, 2005). The FHV B2 protein counteracts the silencing of viral gene expression and acts as a broad-spectrum RNAi inhibitor (Li *et al*, 2002). The B2 protein of a related Nodavirus family member, Nodamura virus (NoV), which is infectious for insect and mammalian hosts, has been shown to block RNAi in mammalian cells (Sullivan & Ganem, 2005). Both the FHV and NoV B2 proteins bind to siRNAs and longer dsRNAs, and may therefore sequester siRNAs and prevent the processing of long dsRNAs into siRNAs by the host RNaseIII-like enzyme Dicer (Lu *et al*, 2005; Sullivan & Ganem, 2005). This mode of inhibition of RNAi is distinct from the strategy used by other viruses. For example, the p19 protein of tombusviruses specifically binds to siRNAs and recognizes their characteristic size (Vargason *et al*, 2003; Ye *et al*, 2003), thus sequestering the products of Dicer and suppressing the silencing effect. The molecular basis of this novel mechanism of RNAi suppression by the 106-residue FHV B2 protein is unknown (Lu *et al*, 2005).

RESULTS

We have determined the three-dimensional structure of the FHV B2 protein using heteronuclear NMR methods. NMR spectra show that the 30 carboxy-terminal residues of full-length B2 are unstructured and highly flexible in solution (supplementary Fig S1 online). For this reason, we solved the structure of a region comprising residues 1–72 of B2.

The B2 protein is a symmetric dimer in solution. The structure is defined well by the NMR data (Fig 1A; Table 1). Each monomer consists of three α-helices (α1: residues 4–23; α2: residues 32–61; α3: residues 64–70), which are arranged in a triangular manner such that the amino- and C terminus of each monomer are in close proximity (Fig 1B,C). Hydrophobic residues stabilize an antiparallel interaction between helices α1 and α2, which are connected by an extended linker between Gly 24 and Pro 31 (Fig 1B). Helix α2 is very elongated and spans 30 residues corresponding to eight helical turns, whereas helix α3 is short and oriented orthogonal to the first two helices.

The dimer is formed by a head-to-tail interaction of the two monomers and involves all three helices (Fig 1C,D). The dimer interface is stabilized by hydrophobic interactions mainly involving aliphatic side chains in helices α1 and α2, as evidenced by inter-monomer nuclear Overhauser effects (NOEs) for residues Leu 7, Ile 8, Met 25, Val 34, Leu 38, Leu 41, Val 52, Met 55, Leu 59, Val 65 and Leu 69 (Fig 1C). An interaction involving Tyr 68 and Ala 30/Pro 31 from separate subunits also contributes to the dimer

European Molecular Biology Laboratory, Meyerhofstrasse 1, 69117 Heidelberg, Germany
[+]Corresponding author. Tel: +49 6221 388 103; Fax: +49 6221 387 306;
E-mail: izaurral@embl.de
[++]Corresponding author. Tel: +49 6221 387 552; Fax: +49 6221 387 306;
E-mail: sattler@embl.de

Received 4 October 2005; revised 18 October 2005; accepted 19 October 2005; published online 4 November 2005

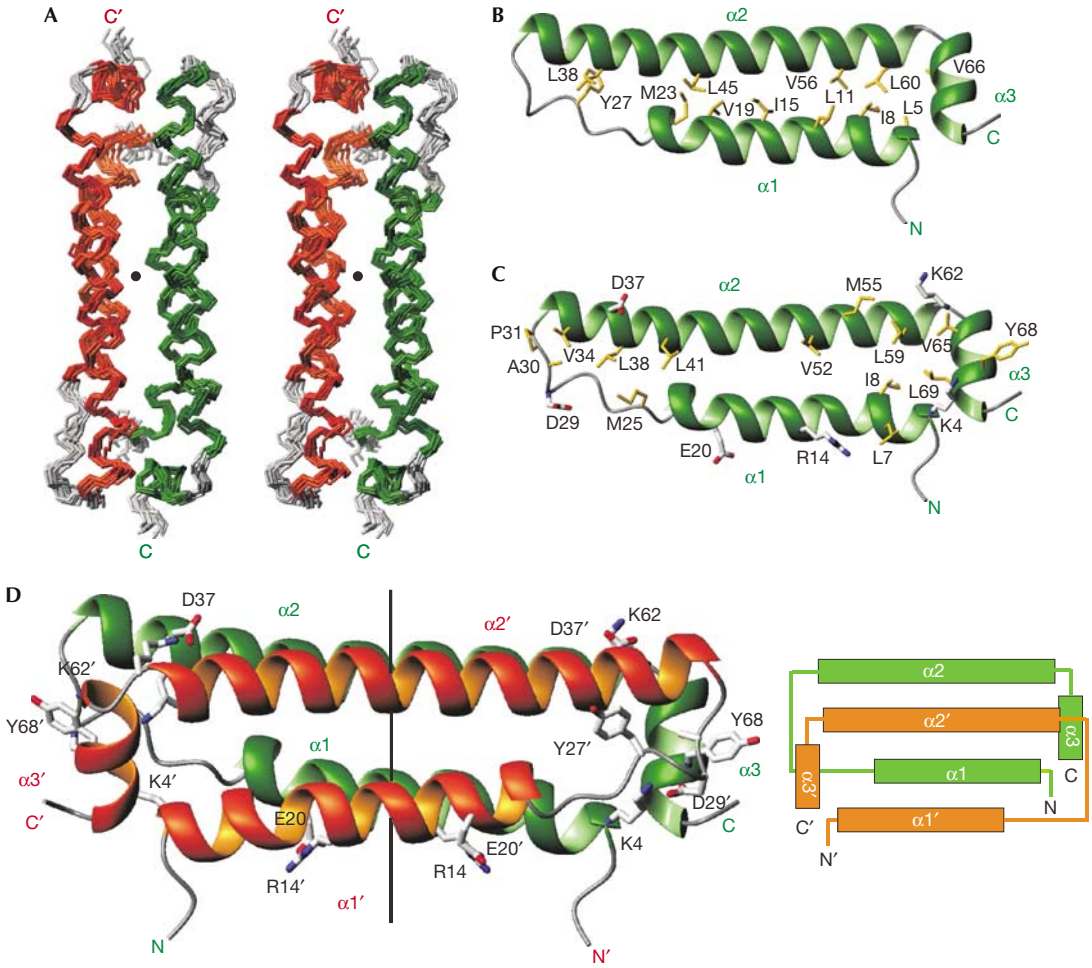

Fig 1 | Solution structure of the flock house virus B2 protein (residues 1–72). (**A**) Stereo view of the ensemble of the ten lowest energy NMR structures of the flock house virus B2 dimer. Secondary structure elements are coloured in green and orange for the two subunits, respectively. The C_2 symmetry axis is indicated by a black dot. (**B**) Ribbon representation of the B2 monomer, in a view rotated by two 90 ° rotations around the *x* and *y* axis compared with (**A**). The subunit is coloured as in (**A**). Side chains of hydrophobic residues involved in intra-monomer interactions are shown and labelled. (**C**) Ribbon representation of the B2 monomer; view and colouring are as in (**B**). Side chains of hydrophobic residues and of charged residues involved in inter-monomer electrostatic contacts contributing to the dimer interface are shown and labelled. (**D**) Ribbon representation of the B2 dimer. Subunits are coloured as in (**A**). The C_2 symmetry axis is shown, as are aromatic residues and side chains of residues involved in electrostatic interactions. The topology of the B2 dimer is shown on the right.

interface, whereas the only other aromatic residue, Tyr 27, is involved in intra-monomer contacts only (Fig 1B). Three inter-monomer electrostatic interactions (Lys 4–Asp 29, Arg 14–Glu 20 and Lys 62–Asp 37) additionally stabilize the dimer interface (Fig 1C,D).

The dimeric conformation of the B2 protein is confirmed by gel filtration (data not shown) and NMR relaxation measurements (Fig 2). Both the average H–N residual dipolar coupling (RDC) values (Tjandra & Bax, 1997) and the average ratio of ^{15}N T1 and T2 relaxation times (T1/T2; Tjandra *et al*, 1997; red lines in Fig 2) in helices α1 and α2 are similar and very different from those in helix α3. This is consistent with the approximately parallel and orthogonal orientations of α1/α2 and α3, respectively, and with the elongated structure of the B2 dimer. The dimerization buries a large surface area (1,500 Å^2 or 25% of the total surface area) in each monomer. Searches in the Protein Data Bank with Dali (Holm & Sander, 1997) or MSDfold (Krissinel & Henrick, 2004) did not show any close structural homologues, indicating that the B2 dimer represents a novel fold. However, the topology of the four-helical bundle formed by α1, α2, α1′ and α2′ in B2 resembles the small dimeric Repressor of primer (Rop) protein (also see below; Banner *et al*, 1987). In contrast to B2, in which all four helices are almost parallel to each other, Rop forms a canonical left-handed four-helical bundle, as reflected in the rather large r.m.s.d. of the atomic backbone coordinates (3.7 Å) between the B2 and Rop dimers.

A recent study showed that recombinant glutathione *S*-transferase-tagged B2 binds to long dsRNA molecules or siRNAs of diverse sequences, but not to single-stranded siRNAs (Lu *et al*, 2005), indicating that B2 binds dsRNA in a size- and sequence-independent manner. We used NMR titration experiments to

Table 1 | Structural statistics for the flock house virus B2 dimer

	〈SA〉*	〈SA〉$_{water-ref}$
Number of nuclear Overhauser effect-derived distance restraints (restraints per monomer)		
All (unambiguous/ambiguous)	2,202/34	
Intra-monomer (unambiguous/ambiguous)	2,073/15	
Inter-monomer (unambiguous/ambiguous)	129/0	
R.m.s.d. (Å) from experimental distance restraints‡		
R.m.s.d. (unambiguous)	0.019 ± 0.003	0.051 ± 0.010
R.m.s.d. (ambiguous)	0.030 ± 0.009	0.037 ± 0.009
Hydrogen bonds (2 × 38 per monomer)	0.032 ± 0.002	0.036 ± 0.004
R.m.s.d. (deg) from experimental torsion restraints§		
R.m.s.d. (55 ϕ/ψ per monomer)	0.42 ± 0.03	0.82 ± 0.05
Q-factor for experimental residual dipolar coupling restraints‖		
$^1D_{HN}$ (22 per monomer)	0.035 ± 0.003	0.041 ± 0.004
Coordinate precision (Å) residues 1–71¶		
N, C^α, C′ (dimer)	0.35 ± 0.06	0.39 ± 0.05
All heavy atoms (dimer)	0.76 ± 0.08	0.80 ± 0.06
N, C^α, C′ (monomer A)	0.31 ± 0.05	0.37 ± 0.04
All heavy atoms (monomer A)	0.74 ± 0.07	0.79 ± 0.06
Structural quality#		
Bad contacts	3.2 ± 1.7	0 ± 0
Ramachandran plot		
Percentage in the most favoured region	94.1 ± 1.7	97.0 ± 1.0
Percentage in the additionally allowed region	5.9 ± 1.7	2.6 ± 1.1

*〈SA〉 is an ensemble of ten lowest-energy solution structures (out of 100 calculated) of the B2 dimer before water refinement. The CNS E_{repel} function was used to simulate van der Waals interactions with an energy constant of 25.0 kcal mol^{-1} Å^{-4} using 'PROLSQ' van der Waals radii (Linge *et al*, 2003); r.m.s.d. for bond lengths, bond angles and improper dihedral angles are 0.00294 ± 0.00008 Å, 0.52 ± 0.01° and 0.558 ± 0.008°. 1 kcal = 4.18 kJ. Non-crystallographic symmetry restraints with an energy constant of 100 kcal mol^{-1} Å^{-2} were used to enforce the dimer symmetry. ‡Distance restraints were used with a soft square-well potential using an energy constant of 50 kcal mol^{-1} Å^2. For hydrogen bonds, distance restraints with bounds of 1.8–2.3 Å (H–O) and 2.8–3.3 Å (N–O) were derived for slowly exchanging amide protons. In the 〈SA〉 structures, 0.2 ± 0.6 distance restraints were violated by more than 0.3 Å. §Dihedral angle restraints derived from TALOS (Cornilescu *et al*, 1999) were applied to ϕ, ψ backbone angles using energy constants of 200 kcal mol^{-1} rad^{-2}. No dihedral angle restraint was violated by more than 5°. ‖Quality factor for the RDC refinement (Cornilescu *et al*, 1998). Residual dipolar couplings were applied with a final energy constant of 0.2 kcal mol^{-1} Hz^{-2} for an alignment tensor with an axial component of 22.7 Hz and a rhombicity of 0.56. ¶Coordinate precision is given as the Cartesian coordinate r.m.s.d. of the ten lowest-energy structures in the NMR ensemble with respect to their mean structure. #Structural quality was analysed using PROCHECK (Laskowski *et al*, 1996).

further characterize the RNA interaction of the B2 dimer. Addition of a 21-mer siRNA duplex induces large changes in the ^{1}H, ^{15}N correlation spectra of B2 (Fig 3A), with signals of the free form disappearing and reappearing at new positions (supplementary Fig S2 online). The slow exchange on the NMR chemical shift timescale between free and bound states is indicative of tight binding with a dissociation constant in the nanomolar range. The titration curve (Fig 3B) and the linewidths in the NMR spectra indicate a 1:1 stoichiometry for the B2 dimer:RNA complex in solution.

The chemical shift perturbations map to the long helices α2/α2′ and also involve residues in α3/α3′, spanning a region of 45 Å in length (Fig 3C,D). Notably, the α2,α2′ helices are highly positively charged, and many lysine and arginine residues are located in this surface. Arg 54, which has been shown to be crucial for dsRNA binding (Lu *et al*, 2005), is located at the centre of this binding interface. Arg 54 and Lys 47 in this region are separated with a spacing of approximately 10 Å (Fig 3C,D), which corresponds to the distance of phosphates across the major groove in an A-form dsRNA conformation. Thus, the exposed arginine and lysine residues may mediate non-sequence-specific electrostatic contacts with the phosphate–sugar backbone of the dsRNA stem. The 1:1 stoichiometry for the B2 dimer:RNA complex and the size of the RNA-binding surface extending across the whole length of the B2 dimer, corresponding to approximately 17-bp A-form dsRNA, indicate that the α2,α2′ helices bind parallel to the stem of the dsRNA helix. Such a mode of dsRNA binding does not recognize the unique 3′ and 5′ ends of an siRNA and is consistent with the ability of B2 to bind to 21-nt siRNA duplexes as well as to dsRNAs of 44–100 nt (Lu *et al*, 2005).

DISCUSSION

The structure of the B2 dimer and the RNA-binding surface mapped by the NMR data are very different from other dsRNA-binding motifs such as the dsRNA-binding domain (dsRBD; Fierro-Monti & Mathews, 2000) or dsRNA-binding zinc-fingers (Lu *et al*, 2003). In the dsRBD, residues of an N-terminal helix and those in loop regions interact with the RNA stem. In the fifth zinc-finger of TFIIIA, a short helix contacts the major groove backbone. Other proteins involved in RNAi also use different modes of RNA recognition (Lingel & Sattler, 2005). The viral p19 protein is, like B2, a dimer but uses an extended β-sheet surface and a small helical motif for binding and measuring the characteristic length of siRNAs (Vargason *et al*, 2003; Ye *et al*, 2003). Interestingly, a four-helical bundle fold is found in the homodimeric Rop protein, a regulator of plasmid copy number in *Escherichia coli* (Banner *et al*, 1987). The predicted binding interface with kissing RNA hairpins comprises an antiparallel pair of the first helix of each

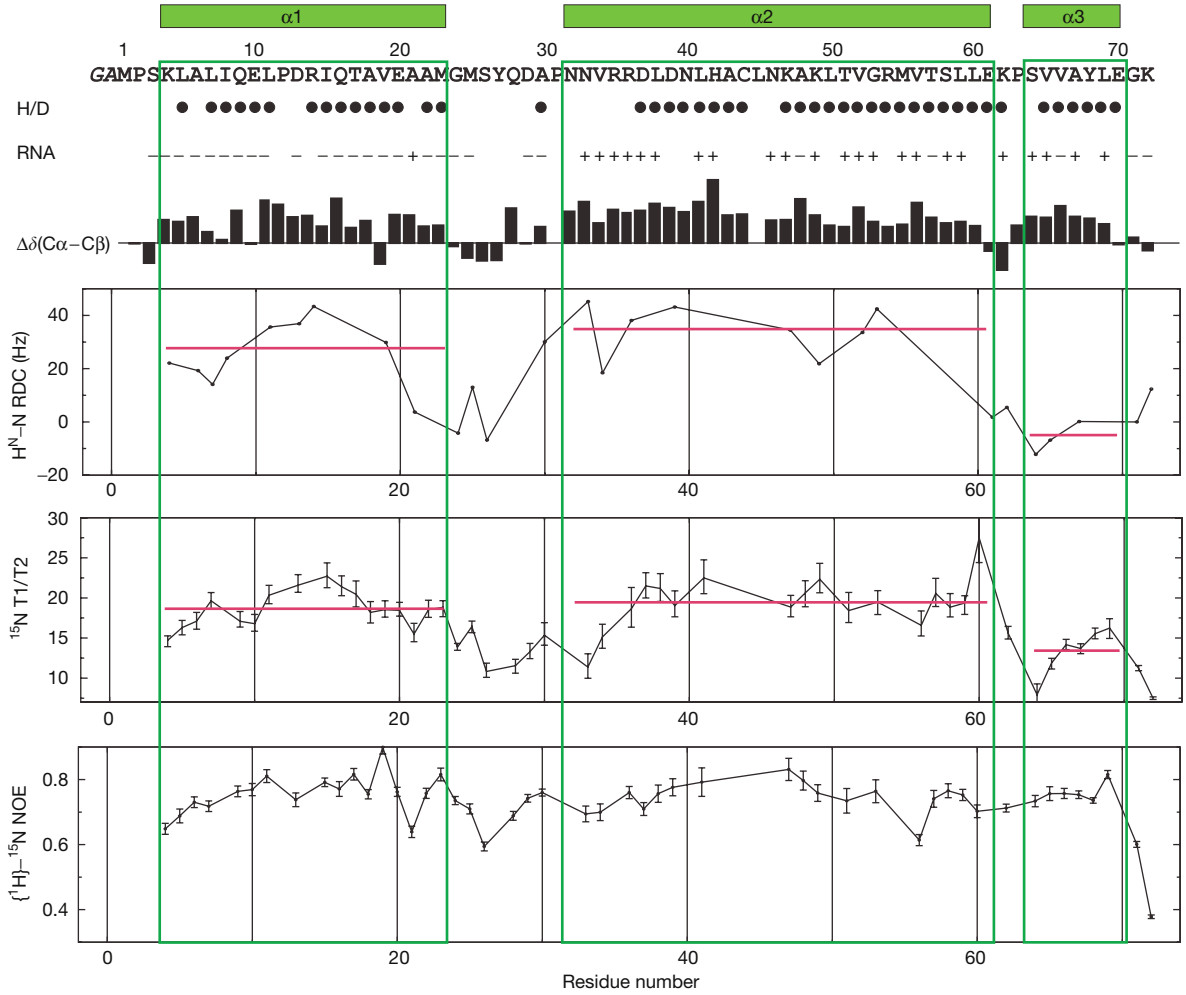

Fig 2 | Summary of NMR data of the flock house virus B2 dimer. The secondary structure is shown above the sequence. Solvent-protected amide protons (slow H/D exchange in NMR measurements) are indicated by filled circles. Residues with and without chemical shift perturbation following double-stranded RNA binding are marked by + and −, respectively. Secondary chemical shifts, $\Delta\delta$(Cα–Cβ), are indicated by black bars. ^{1}H–^{15}N residual dipolar couplings (RDCs) and ^{15}N T1, T2 relaxation data are consistent with the elongated fold of the B2 dimer. Heteronuclear {^{1}H}–^{15}N nuclear Overhauser effect (NOE) data indicate that the protein is very rigid and that there are no regions of increased backbone mobility.

monomer (Predki *et al*, 1995), somewhat resembling the B2 dimeric RNA-binding interface. The N-terminal domain of the influenza virus NS1 protein is a symmetric homodimer formed by two three-helix monomers (Chien *et al*, 1997; Liu *et al*, 1997). Although the NS1 dimer binds dsRNA (Chien *et al*, 2004), the six-helical fold is distinct from that of the FHV B2 dimer. Thus, both the structural elements and the size of the protein–RNA interfaces used by the B2 dimer indicate an unprecedented mode of dsRNA binding.

While this manuscript was under review, the crystal structure of a B2 dimer bound to a palindromic 18 bp RNA duplex was described (Chao *et al*, 2005). Both the monomer and the dimer folds are very similar to our solution structure of the free B2 protein (backbone coordinate r.m.s.d. 1.2/1.3 Å for monomer/dimer). A slightly different orientation of the α3 helices is potentially linked to electrostatic contacts of residues in the preceding linker with the RNA. Notably, the overall high similarity of the structures shows that RNA binding does not induce large conformational changes in the protein. In the protein–RNA complex, the α2/α2′ helices of one B2 dimer are oriented almost parallel to the helical axis of the A-form RNA. Thus, the binding site and stoichiometry are consistent with our NMR data (Fig 3). As expected, the positively charged residues exposed from the RNA-binding surface (Fig 3D) interact with the phosphate–ribose backbone in the RNA helix.

In summary, we describe the structure of the FHV B2 (1–72) protein and characterize its interaction with dsRNA. Our studies show that the helical B2 dimer adopts a novel fold used for dsRNA binding. From biochemical studies (Lu *et al*, 2005; Sullivan & Ganem, 2005) and consistent with the structure of a B2 dimer–dsRNA complex (Chao *et al*, 2005), the RNA binding mode does not discriminate between siRNA duplexes and long dsRNAs, and is thus consistent with a role of B2 in the suppression of RNAi upstream of Dicer (Lu *et al*, 2005).

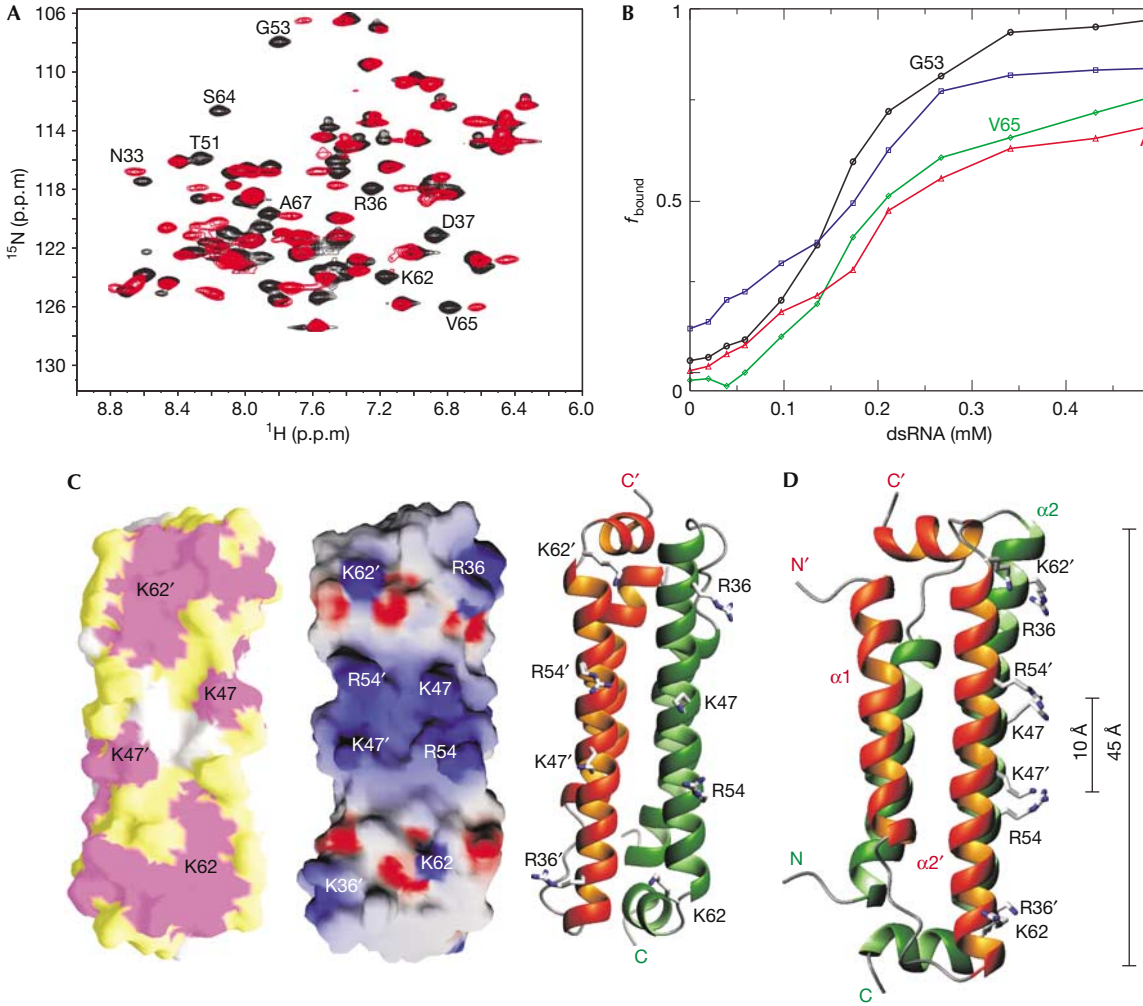

Fig 3 | Binding of flock house virus B2 (1–72) to double-stranded RNA. (**A**) Chemical shift perturbation after addition of a 21-mer short interfering RNA (siRNA) duplex to a ^{2}H-, ^{13}C-, ^{15}N-labelled flock house virus (FHV) B2 dimer. The chemical shifts are monitored in ^{1}H, ^{15}N correlation spectra. The spectrum of the free protein is shown in black and the spectrum after addition of a twofold molar excess of siRNA is shown in red. The dimer concentration was 0.25 mM. (**B**) Titration curves of double-stranded RNA (dsRNA) binding to FHV B2. The fraction of bound protein (f_{bound}) is plotted as a function of ligand concentration. f_{bound} is defined by the signal intensities, $f_{bound} = int_{bound}/(int_{bound} + int_{free})$, where int_{bound} and int_{free} are the peak intensities of the RNA-bound and free NMR signals (supplementary Fig S2 online). The inflection point of the titration curve at equimolar dimer–RNA ratio indicates a 1:1 stoichiometry for the B2 dimer–RNA complex. (**C**) Left: surface representation of the B2 dimer coloured according to chemical shift changes induced following the addition of siRNA (see (**A**)). Residues that are affected/not affected by the RNA addition are shown in magenta/white. Residues that could not be analysed unambiguously because of signal overlap are shown in light yellow. The same orientation as in Fig 1A is shown. Middle: the same surface coloured in blue and red according to positive and negative electrostatic potential, respectively. Right: a ribbon representation in the same orientation. Side chains of residues discussed in the text are shown. (**D**) Proposed interface of the B2 dimer with dsRNA. The B2 dimer is shown rotated by 90° around the *y* axis compared with (**C**). Side chains of lysine and arginine residues in the RNA-binding surface are shown. Distances between these residues and the total length of the RNA-binding surface are indicated.

METHODS

Sample preparation. FHV B2 complementary DNA (Swiss-Prot entry P68831) was amplified by PCR using a random-primed S2 cell cDNA as a template and cloned into the pETM11 vector, which is a derivative of the pET24-d vector (Novagen, Darmstadt, Germany). The recombinant protein was expressed in *E. coli* (BL21-DE3 strain) for 14 h at 25 °C after induction by 0.5 mM isopropyl-β-D-thiogalactoside. For uniform ^{15}N and ^{15}N, ^{13}C labelling, cells were grown in M9 minimal medium supplemented with $^{15}NH_4Cl$ without or with $^{13}C_6$-labelled glucose, respectively. For the preparation of ^{2}H-, ^{13}C-, ^{15}N-labelled sample, the cells were grown in minimal medium prepared with 90% D_2O and supplemented with 10% ^{2}H/^{15}N/^{13}C-rich medium (Silantes, Munich, Germany). Cell lysates were incubated with Ni-NTA Superflow beads (Qiagen, Hilden, Germany). After elution, the fusion protein was cleaved overnight by tobacco etch virus

protease. After a second affinity purification step using Ni-NTA beads, the buffer was exchanged with NMR buffer (50 mM NaP_i, pH 6.3, 50 mM NaCl, 1 mM dithiothreitol) and the protein preparation was concentrated to 0.2–1 mM for NMR experiments. For measurements in D_2O, the protein was lyophilized and redissolved in D_2O.

The sequence of the siRNA used for the titrations was as follows: sense GCA GCA CGA CUU CUU CAA GTT and antisense CUU GAA GAA GUC GUG CUG CTT.

NMR spectroscopy. NMR spectra were acquired at 22 °C on Bruker DRX500, DRX600 and DRX900 spectrometers equipped with cryogenic triple-resonance probes. Spectra were processed with NMRPipe (Delaglio *et al*, 1995) and analysed using NMRVIEW (Johnson & Blevins, 1994). The ^{1}H, ^{13}C and ^{15}N chemical shifts were assigned by standard methods (Sattler *et al*, 1999). Distance restraints were derived from ^{15}N- or ^{13}C-resolved three-dimensional NOESY. H^N–N RDCs were measured using a spin-state-selective ^{1}H, ^{15}N correlation experiment in a dilute liquid crystalline medium (Rückert & Otting, 2000). Restraints for the backbone angles ϕ and ψ were derived from TALOS (Cornilescu *et al*, 1999). Slowly exchanging amide protons were identified from ^{1}H, ^{15}N correlation experiments after redissolving lyophilized protein in D_2O. Stereospecific assignments of leucine and valine methyl groups were obtained using a 10% fractionally ^{13}C-labelled sample, as described (Neri *et al*, 1989).

For NMR titrations, increasing amounts of the 21-mer siRNA were added to a 0.25 mM solution of ^{2}H-, ^{15}N-labelled B2 dimer up to a twofold molar excess. Chemical shifts were monitored in two-dimensional ^{1}H, ^{15}N HSQC experiments. The sigmoidal shape of the binding curves (Fig 3B) may result from slow to intermediate exchange between free and bound conformations on the NMR chemical shift timescale (Feeney *et al*, 1979), but could also indicate a more complex binding behaviour.

^{15}N relaxation (T1, T2 and heteronuclear $\{^{1}H\}$–^{15}N NOE) was measured on a ^{15}N-labelled B2 sample at 295 K and 500 MHz ^{1}H Larmor frequency, as described (Farrow *et al*, 1994). The different T1/T2 ratios for helices α1 and α2 compared with helix α3 are consistent with the elongated structure of the B2 dimer, and indicate a considerable degree of anisotropy of the rotational diffusion tensor (Tjandra *et al*, 1997). Analysis of the data using TENSOR (Dosset *et al*, 2000) indicates a prolate diffusion tensor with an axial ratio of 1:1.6 and an overall tumbling correlation time of 15.5 ns. The relaxation data fit well to the elongated dimer structure, although the average T2 values (trimmed mean $T2 = 42$ ms) are shorter than expected, indicating further exchange broadening for many amide protons.

Structure calculation. The experimentally determined distance and dihedral and dipolar coupling restraints (Table 1) were applied in a simulated annealing protocol using ARIA (Linge *et al*, 2001) and CNS (Brünger *et al*, 1998). Non-crystallographic symmetry restraints were used to enforce the dimer symmetry. In a first step, all NOEs were entered with a fourfold ambiguity, that is, two intra-monomer and two inter-molecular assignments. After convergence, the NOEs were assigned unambiguously (when possible) as inter- or intra-monomer contacts. Symmetrically unambiguous and ambiguous peak lists were created and used in a final structure calculation for refined distance calibrations. The final ensemble of NMR structures was refined in a shell of water molecules (Linge *et al*, 2003). Structural quality was analysed using PROCHECK (Laskowski *et al*, 1996). Ribbon and surface representations were prepared with MOLMOL (Koradi *et al*, 1996) and GRASP (Nicholls *et al*, 1991), respectively.

Protein Data Bank accession numbers. The coordinates and NMR data for the B2 dimer structure have been deposited at the Protein Data Bank under accession number 2B9Z.

Supplementary information is available at *EMBO reports* online (http://www.emboreports.org).

ACKNOWLEDGEMENTS

We thank M. Nilges (Institut Pasteur, Paris) for help with structure calculations and C. Mackereth and D. Thomas for a critical reading of the manuscript. High-field NMR measurement time granted by the German Research Foundation (DFG) at the Biomolecular Magnetic Resonance Centre in Frankfurt (Germany) is acknowledged. This study was supported by the European Molecular Biology Organization (EMBO), the DFG, the European Union (STREP FSG-V-RNA) and the Human Frontier Science Program Organization.

Competing interests statement

The authors declare that they have no competing financial interests.

REFERENCES

Banner DW, Kokkinidis M, Tsernoglou D (1987) Structure of the ColE1 rop protein at 1.7 Å resolution. *J Mol Biol* **196:** 657–675

Brünger AT *et al* (1998) Crystallography & NMR system: a new software suite for macromolecular structure determination. *Acta Crystallogr D* **54:** 905–921

Chao JA, Lee JH, Chapados BR, Debler EW, Schneemann A, Williamson JR (2005) Dual modes of RNA-silencing suppression by Flock House virus protein B2. *Nat Struct Mol Biol* (Epub ahead of print) doi:10.1038/nsmb1005

Chien CY, Tejero R, Huang Y, Zimmerman DE, Rios CB, Krug RM, Montelione GT (1997) A novel RNA-binding motif in influenza A virus non-structural protein 1. *Nat Struct Biol* **4:** 891–895

Chien CY, Xu Y, Xiao R, Aramini JM, Sahasrabudhe PV, Krug RM, Montelione GT (2004) Biophysical characterization of the complex between double-stranded RNA and the N-terminal domain of the NS1 protein from influenza A virus: evidence for a novel RNA-binding mode. *Biochemistry* **43:** 1950–1962

Cornilescu G, Marquardt JL, Ottiger M, Bax A (1998) Validation of protein structure from anisotropic carbonyl chemical shifts in a dilute liquid crystalline phase. *J Am Chem Soc* **120:** 6836–6837

Cornilescu G, Delaglio F, Bax A (1999) Protein backbone angle restraints from searching a database for chemical shift and sequence homology. *J Biomol NMR* **13:** 289–302

Delaglio F, Grzesiek S, Vuister G, Zhu G, Pfeifer J, Bax A (1995) NMRPipe: a multidimensional spectral processing system based on UNIX Pipes. *J Biomol NMR* **6:** 277–293

Dosset P, Hus JC, Blackledge M, Marion D (2000) Efficient analysis of macromolecular rotational diffusion from heteronuclear relaxation data. *J Biomol NMR* **16:** 23–28

Farrow NA, Muhandiram R, Singer AU, Pascal SM, Kay CM, Gish G, Shoelson SE, Pawson T, Forman-Kay JD, Kay LE (1994) Backbone dynamics of a free and phosphopeptide-complexed Src homology 2 domain studied by ^{15}N NMR relaxation. *Biochemistry* **33:** 5984–6003

Feeney J, Batchelor JG, Albrand JP, Roberts GCK (1979) The effects of intermediate exchange processes on the estimation of equilibrium constants by NMR. *J Magn Reson* **33:** 519–529

Fierro-Monti I, Mathews MB (2000) Proteins binding to duplexed RNA: one motif, multiplefunctions. *Trends Biochem Sci* **25:** 241–246

Holm L, Sander C (1997) Dali/FSSP classification of three-dimensional protein folds. *Nucleic Acids Res* **25:** 231–234

Johnson BA, Blevins RA (1994) NMRView: a computer program for the visualization and analysis of NMR data. *J Biomol NMR* **4:** 603–614

Johnson KN, Johnson KL, Dasgupta R, Gratsch T, Ball LA (2001) Comparisons among the larger genome segments of six nodaviruses and their encoded RNA replicases. *J Gen Virol* **82:** 1855–1866

Koradi R, Billeter M, Wüthrich K (1996) MOLMOL: a program for display and analysis of macromolecular structures. *J Mol Graph* **14:** 51–55

Krissinel E, Henrick K (2004) Secondary-structure matching (SSM), a new tool for fast protein structure alignment in three dimensions. *Acta Crystallogr D* **60:** 2256–2268

Laskowski RA, Rullmannn JA, MacArthur MW, Kaptein R, Thornton JM (1996) AQUA and PROCHECK-NMR: programs for checking the quality of protein structures solved by NMR. *J Biomol NMR* **8:** 477–486

Li H, Li WX, Ding SW (2002) Induction and suppression of RNA silencing by an animal virus. *Science* **296:** 1319–1321

Linge JP, O'Donoghue SI, Nilges M (2001) Automated assignment of ambiguous nuclear overhauser effects with ARIA. *Methods Enzymol* **339:** 71–90

Linge JP, Williams MA, Spronk CA, Bonvin AM, Nilges M (2003) Refinement of protein structures in explicit solvent. *Proteins* **50:** 496–506

Lingel A, Sattler M (2005) Novel modes of protein–RNA recognition in the RNAi pathway. *Curr Opin Struct Biol* **15:** 107–115

Liu J, Lynch PA, Chien CY, Montelione GT, Krug RM, Berman HM (1997) Crystal structure of the unique RNA-binding domain of the influenza virus NS1 protein. *Nat Struct Biol* **4:** 896–899

Lu D, Searles MA, Klug A (2003) Crystal structure of a zinc-finger–RNA complex reveals two modes of molecular recognition. *Nature* **426:** 96–100

Lu R, Maduro M, Li F, Li HW, Broitman-Maduro G, Li WX, Ding SW (2005) Animal virus replication and RNAi-mediated antiviral silencing in *Caenorhabditis elegans*. *Nature* **436:** 1040–1043

Neri D, Szyperski T, Otting G, Senn H, Wüthrich K (1989) Stereospecific nuclear magnetic resonance assignments of the methyl groups of valine and leucine in the DNA-binding domain of the 434 repressor by biosynthetically directed fractional ^{13}C labeling. *Biochemistry* **28:** 7510–7516

Nicholls A, Sharp KA, Honig B (1991) Protein folding and association: insights from the interfacial and thermodynamic properties of hydrocarbons. *Proteins Struct Funct Genet* **11:** 281–296

Plasterk RH (2002) RNA silencing: the genome's immune system. *Science* **296:** 1263–1265

Predki PF, Nayak LM, Gottlieb MB, Regan L (1995) Dissecting RNA–protein interactions: RNA–RNA recognition by Rop. *Cell* **80:** 41–50

Roth BM, Pruss GJ, Vance VB (2004) Plant viral suppressors of RNA silencing. *Virus Res* **102:** 97–108

Rückert M, Otting G (2000) Alignment of biological macromolecules in novel nonionic liquid crystalline media for NMR experiments. *J Am Chem Soc* **122:** 7793–7797

Sattler M, Schleucher J, Griesinger C (1999) Heteronuclear multidimensional NMR experiments for the structure determination of proteins in solution employing pulsed field gradients. *Prog NMR Spectrosc* **34:** 93–158

Sullivan CS, Ganem D (2005) A virus-encoded inhibitor that blocks RNA interference in mammalian cells. *J Virol* **79:** 7371–7379

Tjandra N, Bax A (1997) Direct measurement of distances and angles in biomolecules by NMR in a dilute liquid crystalline medium. *Science* **278:** 1111–1114

Tjandra N, Garrett DS, Gronenborn AM, Bax A, Clore GM (1997) Defining long range order in NMR structure determination from the dependence of heteronuclear relaxation times on rotational diffusion anisotropy. *Nat Struct Biol* **4:** 443–449

Vargason JM, Szittya G, Burgyan J, Tanaka Hall TM (2003) Size selective recognition of siRNA by an RNA silencing suppressor. *Cell* **115:** 799–811

Voinnet O (2005) Induction and suppression of RNA silencing: insights from viral infections. *Nat Rev Genet* **6:** 206–220

Ye K, Malinina L, Patel DJ (2003) Recognition of small interfering RNA by a viral suppressor of RNA silencing. *Nature* **426:** 874–878